Coded aperture x-ray imaging of high power laser-plasma interactions on the Vulcan Laser System

R. Heathcote, A. Anderson-Asubonteng, R. J. Clarke, M. P. Selwood, C. Spindloe and N. Booth

Published version information

Citation: RI Heathcote et al. "Coded aperture x-ray imaging of high power laser-plasma interactions on the Vulcan Laser System." Proceedings of SPIE, vol. 10763 (2018): 107630U. Is in **Radiation Detectors in Medicine, Industry, and National Security XIX**, proceedings of SPIE Optical Engineering + Applications 2018, San Diego, California, USA, 19-23 Aug 2018.

DOI: 10.1117/12.2319380

PROCEEDINGS OF SPIE

SPIEDigitalLibrary.org/conference-proceedings-of-spie

Coded aperture x-ray imaging of high power laser-plasma interactions on the Vulcan Laser System

R. Heathcote, A. Anderson-Asubonteng, R. J. Clarke, M. P. Selwood, C. Spindloe, et al.

R. Heathcote, A. Anderson-Asubonteng, R. J. Clarke, M. P. Selwood, C. Spindloe, N. Booth, "Coded aperture x-ray imaging of high power laser-plasma interactions on the Vulcan Laser System," Proc. SPIE 10763, Radiation Detectors in Medicine, Industry, and National Security XIX, 107630U (11 September 2018); doi: 10.1117/12.2319380

SPIE.

Event: SPIE Optical Engineering + Applications, 2018, San Diego, California, United States

Coded Aperture X-ray Imaging of High Power Laser-Plasma interactions on the Vulcan Laser System

R. Heathcote*[a], A. Anderson-Asubonteng[a], R. J. Clarke[a], M. P. Selwood[a,b], C. Spindloe[a] and N. Booth[a]

[a]Central Laser Facility, Science and Technology Facilities Council, Rutherford Appleton Laboratory, Harwell Oxford, Didcot, Oxfordshire, United Kingdom

[b]Department of Physics, University of York, Heslington, York, United Kingdom

ABSTRACT

In this paper we demonstrate the implementation of a modified uniformly redundant array (MURA) coded aperture in the x-ray imaging of high power laser produced plasma. We detail the process of design and manufacture of a self-supporting tantalum coded aperture with ~ 50% open area to work in the 1-25 keV x-ray regime. The advantage of using a coded aperture imaging system in this high noise environment in comparison to a standard pinhole aperture is its larger solid angle and increased signal to noise. The increased solid angle allows the aperture and detector to be placed at a further distance from the interaction point. This is beneficial as it reduces the mechanics in the close proximity of the often crowded interaction region and moves the detector which can include sensitive electronics further away from the source of EMP, hard x-rays and secondary sources generated in the interaction. Here we present initial data taken on an experiment using the Vulcan Petawatt Laser at the Central Laser Facility of a prototype x-ray imager.

Keywords: Coded Aperture Imaging, X-ray imaging, Pinhole Camera, High Power Laser, Laser Plasma Interactions, Vulcan Petawatt, Central Laser Facility

1. INTRODUCTION

The family of uniformly redundant array coded apertures have been around for many decades [1]. Successfully exploited in Astronomy for X-ray and gamma ray imaging of sources [2] they have gone on to be used in many fields including the nuclear industry, medical physics [3] and with synchrotron sources [4]. However they are not a commonly used diagnostic in high power lasers for soft x-ray (1-25 keV) measurements from much beyond their initial development in the late 1970's and early 1980's [5][6], possibly in part due to the complexity of manufacture of the micro-scale structured masks and decoding process as well as the development of other techniques. The continued increase in computing power and the development of new manufacturing processes has meant that it has again become viable to develop a diagnostic for soft x-ray imaging using uniformly redundant array coded apertures.

A high power laser-produced plasma interaction produces a harsh environment of high energy particles, photons and electromagnetic pulses (EMP)[7][8]. Proximity to this can lead to high noise data, failed shots and at worst damaged detectors. Depending on the experiment the interaction region can also be crowded with mechanics such as plasma mirrors and cryogenic target systems, as well as other diagnostics that can take up a large solid angle of the target interaction region.

Common imaging in the soft x-ray region of emission of laser produced plasma at the Central Laser Facility is performed with pinhole cameras and K-alpha crystal imagers. Pinhole cameras are very simple and effective but can suffer from signal to noise problems due to the opacity of the pinhole substrate to hard x-rays reducing the contrast of the image. To gain enough signal through the small numerical aperture of the pinhole they often have to sit very close to the interaction region. K-alpha crystal imagers are useful in that they have a relatively large working distance and numerical aperture compared to a pinhole [9][10] and allow for the detector to sit away from the interaction region. They are however designed to image a narrow range of photon energies of specific atomic transitions in certain elements, such as copper and titanium, so cannot be utilized for all materials.

*robert.heathcote@stfc.ac.uk

Radiation Detectors in Medicine, Industry, and National Security XIX, edited by Gary P. Grim, Lars R. Furenlid, H. Bradford Barber, Proc. of SPIE Vol. 10763, 107630U · © 2018 SPIE
CCC code: 0277-786X/18/$18 · doi: 10.1117/12.2319380

Coded apertures have the potential to be produced with pinhole scale holes but with a large solid angle to allow the detector to sit further away from the interaction. The motivation of this work is to produce a relatively low cost imager that has the ability to have a larger working distance and to allow the detector to be placed further away from the interaction point.

2. THEORETICAL REVIEW

2.1 Coded Aperture

Coded aperture imaging can be seen as evolution of pinhole imaging, however unlike pinhole imaging where the image formed is a likeness of the object, a coded aperture image is a convolution of the object and the aperture. Post processing is required to get back to the likeness of the object from the formed image. In this case the detected signal D from the object S is convolved with the aperture mask A.

$$D = S * A \tag{1}$$

To retrieve a likeness of the object S' from detected signal D then it must be correlated with a decoding array G which is derived from A:

$$S' = D * G \tag{2}$$

Substituting equation 1 in to equation 2 gives:

$$S' = (S * A) * G \tag{3}$$

By design, G is the correlation inverse of A,

$$A * G \equiv \delta \tag{4}$$

and therefore, gives a delta function system point spread response δ. Substituting this in to equation 3 results in the formation of the image S' from the object signal S.

The design in this paper is based on the Modified Uniformly Redundant Array (MURA). The MURA is a binary coded aperture design derived by Gottesman and Fenimore [11] that has many advantages over other previous aperture designs in that the scale is based on prime numbers and so a wide range of aperture sizes can easily be derived. The post processing decoding array is also uni-modular and is based on the mask itself.

The square pattern of the mask is based on quadratic residues of a prime number p which defines the aperture size. The binary array of transparent and opaque sections are in a checkerboard arrangement.

$$A_{ij}\begin{cases} 0 \text{ if } i = 0, \\ 1 \text{ if } j = 0, i \neq 0, \\ 1 \text{ if } C_i C_j = +1, \\ 0 \text{ otherwise} \end{cases} \tag{5}$$

$$C_{i,j}\begin{cases} +1 \text{ if } i,j \text{ is a quadratic residue modulo p} \\ -1 \text{ if } i,j \text{ is not a quadratic residue modulo p} \end{cases} \tag{6}$$

To make the array in to a usable coded aperture, the array is transformed cyclically as proscribed in reference [11] to bring $i,j = 0$ to the center of the mask. To allow the image of the mask to be projected such that $i,j = 0$ can be projected to the corners of the detector without vignetting, the pattern of the mask is repeated around the $p \times p$ array such that the resultant mask is $2p-1$ tall and wide. Figure 1 shows an example of a mask of $p = 43$ and can be seen that the open area of the mask is almost equal to that of the enclosed regions.

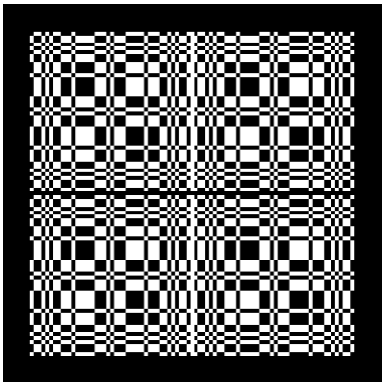

Figure 1. MURA Coded Aperture mask with $p = 43$ scale size.

As mentioned earlier the decoding array G is derived from A by:

$$G_{ij}\begin{cases}+1 \text{ if } i+j=0,\\ +1 \text{ if } A_{ij}=1,(i+j\neq 0),\\ -1 \text{ if } A_{ij}=0,(i+j\neq 0),\end{cases} \tag{7}$$

This produces a uni-modular array that is the inverse correlation of A.

2.2 Resolution and field of view

The resolution of the coded aperture depends on the pixel/minimum aperture size of the array and obeys the same rules of pinhole imaging. Therefore, to image the emission from a laser-plasma interaction the resolution has to be on the sub 100 μm scale. The resolution R of the aperture mask is:

$$R = \Delta A_{min}\left(1+\frac{1}{M}\right) \tag{8}$$

Where ΔA_{min} is the smallest aperture/pixel size within the array A, and M is the magnification of the image defined as $M=v/u$ from Figure 2.

The field of view is limited by the magnification and detector size in the same way as a pinhole camera. The added complication in selecting the correct aperture size is that to maximize the signal strength a $p \times p$ sized portion of the mask A should project to fill the detector. For ideal conditions the aperture mask should be:

$$A = \Delta A_{min}\left(\frac{2D}{n(M+1)}-1\right) \tag{9}$$

in size. Where D and n are the detector and detector pixel size respectively. The resolution of the detector should be sufficient to resolve each aperture pixel and adds to the resolution limit with n/M.

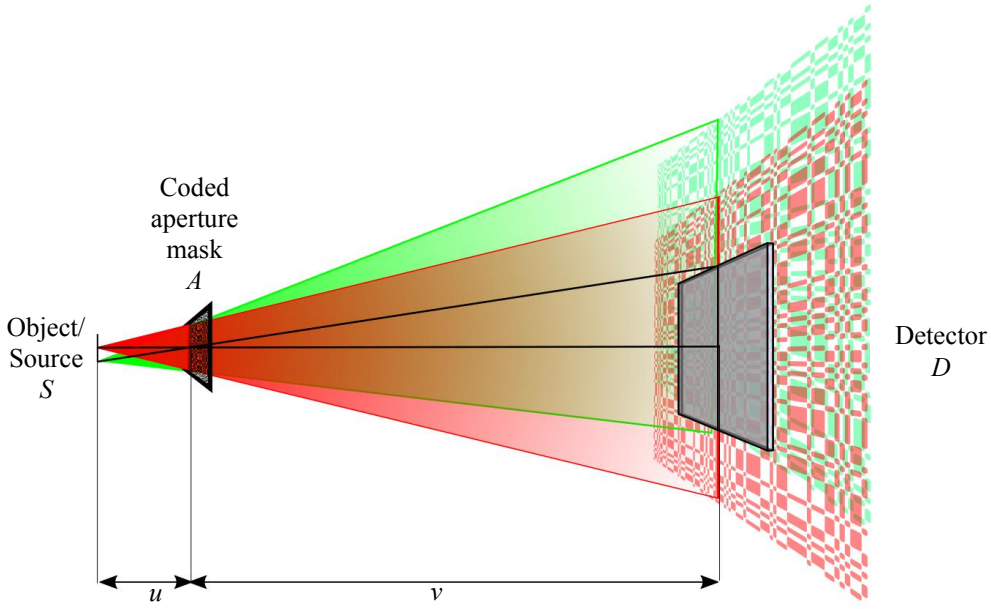

Figure 2. Schematic diagram of setup.

For the decoding function to reproduce the image of the object source the decoding mask *G* must be scaled to match the size of the projected image of the aperture *A* on the detector plane. A scaling factor may also need to be applied to account for differences in detector and aperture pixel size.

2.3 Decoding process

The process of correlating the decoding mask to the detected image is done by transforming them both into the Fourier domain via Fast Fourier Transform (FFT) and then multiplying them together. The resultant image is then inverse Fourier transformed to produce the final image. A MATLAB code was produced de-convolve the obtained images.

3. DETAIL OF DESIGN

The design of the MURA aperture is made up of opaque and transparent regions. The approach used in this paper to create the aperture mask was to remove material from an opaque substrate with the use of laser machining. The MURA design in its nature is not self-supporting as the opaque sections only meet at the corners. To make a self-supporting aperture material was left at the corners to form bridges that allow the aperture to be held together while maintaining a high proportion of open area. The bridges are formed by rounding the corners of the open apertures (Figure 3).

The coded aperture was designed to work in the soft x-ray region of 1–25 keV. A substrate of 100 μm tantalum was chosen based on its transmission properties in this spectral region (Figure 4).

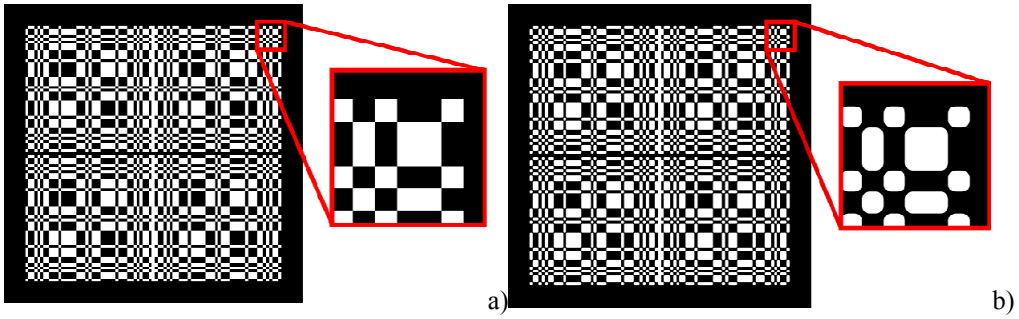

Figure 3. Comparison of a) standard MURA design with b) modified self-supporting MURA design with ratio of 0.36 corner radii to minimum aperture width.

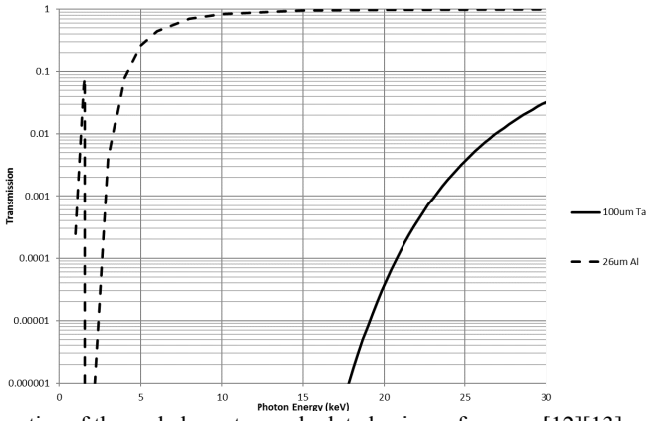

Figure 4. Transmission properties of the coded aperture calculated using references [12][13].

The laser used for machining was a Coherent Avia operating at a wavelength of 355 nm, running at up to 200 kHz with maximum average power of 20 W and with a pulse length of 30 ns. The minimum corner radius achievable with this system was measured to be 18 µm. It was determined that the minimum aperture for this design would be 50 µm. which would give a minimum bridge width of ~15 µm. Given a minimum aperture pixel size of 50 µm it was decided to produce a mask of p=43 which produces a mask 85 pixels or 4.25 mm square.

The results of the laser machining can be seen in Figure 5 and 6. The quality of the laser machining to first order is good but under closer inspection it does not exactly meet the intended design specification. The profile of the machined walls taper through the depth of the substrate material. This resulted in smaller holes than designed as well as a slight size discrepancy between the orthogonal axes. This effect will reduce the spatial resolution although this was not fully explored through the design and manufacture process.

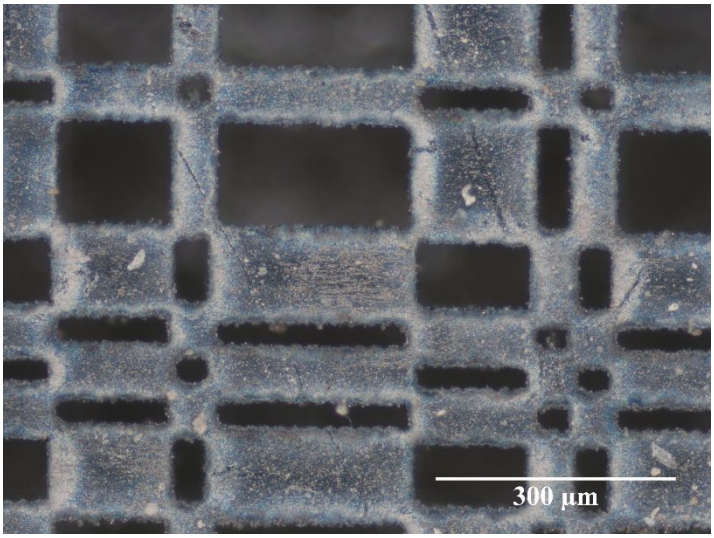

Figure 5. High resolution microscope image of laser machined aperture.

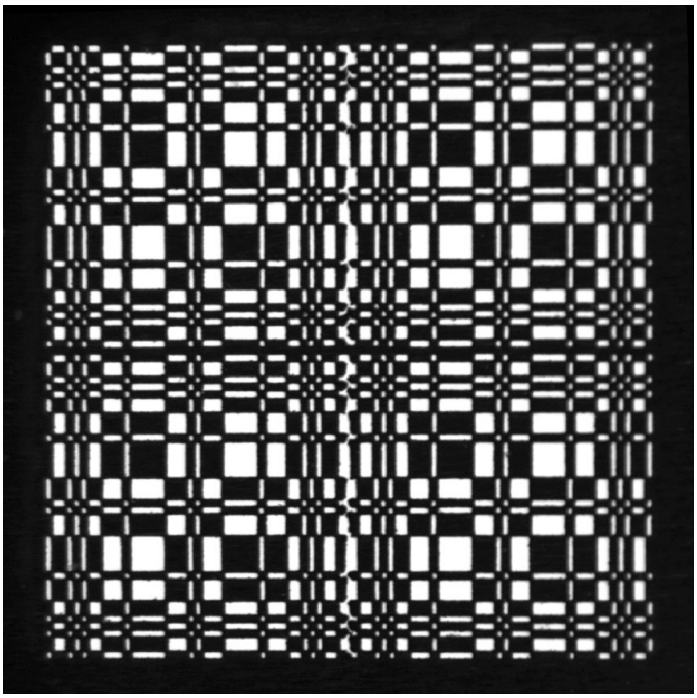
Figure 6. Low resolution microscope image of laser machined 4.25×4.25 mm aperture.

4. EXPERIMENT RESULTS

The experiment was performed on the Vulcan Petawatt facility with the majority of the shots running at ~450 J in ~600 fs from the laser using a high contrast system formed of a double plasma mirror setup delivering ~150 J on target. The targets of the experiment were predominately 100 × 100 μm^2 Polysulphone foils of at 10 and 25 μm thicknesses. For this prototype imager the detector was chosen to be Fujifilm SR Imageplate scanned at 50 μm resolution. The coded aperture was mounted to an existing pinhole camera body and the magnification was set to 10x with a working distance of 75 mm from the interaction. Filtering of 26 μm Aluminum was used as an optical light block as well as to attenuate the x-ray signal. A standard pinhole camera using Fujifilm SR Imageplate working at 20x with a 25 μm Tantalum pinhole, a 25 μm Beryllium filter and a working distance of 25 mm was also used for comparison. An example of the data obtained from both can be seen in Figure 7.

The pinhole camera measured an x-ray source size of ~ 30 μm FWHM which is consistent with the resolution limit of that instrument. The coded aperture measured the x-ray source to be 70 μm FWHM which is larger than the expected calculated detector resolution limit of 60 μm FWHM. This can be attributed to the coded aperture manufacture not meeting the intended design as mentioned in the previous section. Cross correlating the decoding function *G* with the optical microscope image of the aperture mask, as well as a simulation of the of the observed mask, both scaled to the system give an effective resolution limit size of 70 μm.

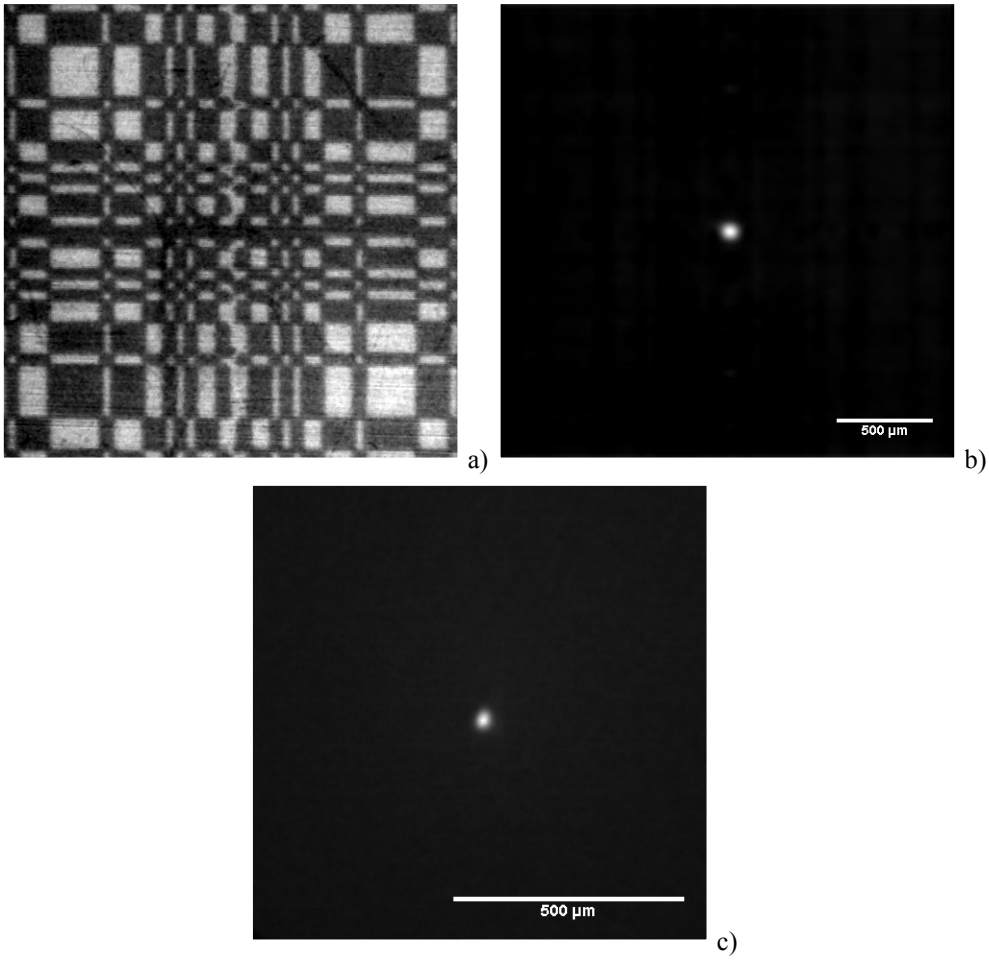

a) b) c)

Figure 7 a) Raw X-ray image captured with coded aperture b) Processed image of X-ray coded aperture c) Pinhole camera captured X-ray image.

5. CONCLUSION AND FUTURE DEVELOPMENTS

The aim of this project was to develop the knowledge and skills to design and manufacture coded apertures for use in the field of high power laser interactions. Here we demonstrate a prototype imager using a laser machined self-supporting MURA coded aperture applied to the soft x-ray emission from a high power laser interaction. This initial prototype has holes that are too large for resolving detail from the short pulse interaction and a planned development is to design and manufacture a coded aperture mask with smaller holes to increase the resolution. The prototype design will be used to measure the emission from larger sources such as those from the long pulse beam interactions in the facility. The aim is to continue this development and move to active capture with either a direct detection x-ray CCD or phosphor coupled system.

6. ACKNOWLEDGEMENTS

The authors gratefully acknowledge the expert assistance of the CLF Vulcan operations and technical support teams. Data associated with research published in this paper can be accessed via http://dx.doi.org/10.5286/edata/718.

REFERENCES

[1] Fenimore, E. E., and Cannon, T. M., "Coded aperture imaging with uniformly redundant arrays," Appl. Opt. 17(3), 337 (1978)
[2] Caroli, E., Stephen, J. B., Di Cocco, G., Natalucci, L., Spizzichino, A., "Coded aperture imaging in X- and gamma-ray astronomy," Space Sci. Rev. 45, 349 (1987)
[3] Cieślak, M. J., Gamage, K. A. A., Glover, R., "Coded-aperture imaging systems: Past, present and future development – A review," Radiat. Meas. 92, 59 (2016)
[4] Haboub, A., Macdowell, A. A., Marchesini, S., Parkinson, D. Y., "Coded aperture imaging for fluorescent x-rays," Rev. Sci. Instrum. 85, 063704 (2014)
[5] Fenimore, E. E., Cannon, T. M., Van Hulsteyn, D. B., Lee, P., "Uniformly redundant array imaging of laser driven compressions: preliminary results,", Appl. Opt. 18, 945 (1979)
[6] Yamanaka, C., Yamanaka, M., Niki, H., Yamada, A., Yamamoto, Y., Yamanaka, T., "A URA Coded Aperture Camera for the Inertial Confinement Fusion Experiments," IEEE Trans. Nucl. Sci. 31(1), 490 (1984)
[7] Mead, M.J.; Neely, D.; Gauoin, J.; Heathcote, R.; Patel, P., "Electromagnetic pulse generation within a petawatt laser target chamber", Rev. Sci. Instrum. 75, 4225 (2004)
[8] Bradford, P., Woolsey, N. C., Scott, G. G., Liao, G., Liu, H., Zhang, Y., Zhu, B., Armstrong, C., Astbury, S., Brenner, C., Brummitt, P., Consoli, F., East, I., Gray, R., Haddock, D., Huggard, P., Jones, P. J. R., Montgomery, E., Musgrave, I., Oliveira, P., Rusby, D R., Spindloe, C., Summers, B., Zemaityte, E., Zhang, Z., Li, Y., Mckenna, P., Neely, D., "EMP control and characterization on high-power laser systems", High Power Laser Sci. Eng. 6, e21 (2018)
[9] Koch, J. A., Aglitskiy, Y., Brown, C., Cowan, T., Freeman, R., Hatchett, S., Holland, G., Key, M., MacKinnon, A., Seely, J., Snavely, R., Stephens, R., "4.5- and 8-keV emission and absorption x-ray imaging using spherically bent quartz 203 and 211 crystals (invited),"Rev. Sci. Instrum. 75, 2130 (2003)
[10] King, J. A., Akli, K., Snavely, R. A., Zhang, B., Key, M. H., Chen, C. D., Chen, M., Hatchett, S. P., Koch, J. A., MacKinnon, A. J., Patel, P. K., Phillips, T., Town, R. P. J., Freeman, R. R., Borghesi, M., Romagnani, L., Zepf, M., Cowan, T., Stephens, R., Lancaster, K. L., Murphy, C. D., Norreys, P., Stoeckl, C., "Characterization of a picosecond laser generated 4.5keV TiK-alpha source for pulsed radiography," Rev. Sci. Instrum. 76, 076102 (2005)
[11] Gottesman, S. R., Fenimore, E., "New family of binary arrays for coded aperture imaging," Appl. Opt. 28(20), 4344 (1989)
[12] Henke, B.L., Gullikson, E.M., Davis, J.C., "X-ray interactions: photoabsorption, scattering, transmission, and reflection at E=50-30000 eV, Z=1-92," At. Data Nucl. Data Tables 54 (2), 181-342 (July 1993). http://henke.lbl.gov/optical_constants (July 2017)
[13] Hubbell, J.H., Seltzer, S.M., "Tables of X-Ray Mass Attenuation Coefficients and Mass Energy-Absorption Coefficients," (version 1.4) (2004). http://physics.nist.gov/xaamdi (July 2017)